

# Rapid MR elastography of the liver for subsecond stiffness sampling

Matthias Anders<sup>1</sup> | Tom Meyer<sup>1</sup> | Carsten Warmuth<sup>1</sup> | Josef Pfeuffer<sup>2</sup> |  
Heiko Tzschaetzsch<sup>1</sup> | Helge Herthum<sup>3</sup> | Mehrgan Shahryari<sup>1</sup> |  
Katja Degenhardt<sup>4</sup> | Oliver Wieben<sup>5,6</sup> | Sebastian Schmitter<sup>4</sup> |  
Jeanette Schulz-Menger<sup>7,8,9,10</sup> | Tobias Schaeffter<sup>4,11</sup> | Juergen Braun<sup>12</sup> |  
Ingolf Sack<sup>1</sup>

## Correspondence

Ingolf Sack, Department of Radiology,  
Charité–Universitätsmedizin Berlin,  
Corporate Member of Freie Universität  
Berlin and Humboldt-Universität zu  
Berlin, Charitéplatz 1, 10117 Berlin,  
Germany.  
Email: [ingolf.sack@charite.de](mailto:ingolf.sack@charite.de)

## Funding information

BIOQIC, Grant/Award Numbers:  
CRC1340, RTG2260; German research  
foundation (DFG)

## Abstract

**Purpose:** Depicting the stiffness of biological soft tissues, MR elastography (MRE) has a wide range of diagnostic applications. The purpose of this study was to improve the temporal resolution of 2D hepatic MRE in order to provide more rapid feedback on the quality of the wavefield and ensure better temporal sampling of respiration-induced stiffness changes.

**Methods:** We developed a rapid MRE sequence that uses 2D segmented gradient-echo spiral readout to encode 40 Hz harmonic vibrations and generate stiffness maps within 625 ms. We demonstrate the use of this technique as a rapid test for shear wave amplitudes and overall MRE image quality and as a method for monitoring respiration-induced stiffness changes in the liver in comparison to 3D MRE and ultrasound-based time-harmonic elastography.

**Results:** Subsecond MRE allowed monitoring of increasing shear wave amplitudes in the liver with increasing levels of external stimulation within a single breath-hold. Furthermore, the technique detected respiration-induced changes in liver stiffness with peak values ( $1.83 \pm 0.22$  m/s) at end-inspiration, followed by softer values during forced abdominal pressure ( $1.60 \pm 0.22$  m/s) and end-expiration ( $1.49 \pm 0.22$  m/s). The effects of inspiration and expiration were confirmed by time-harmonic elastography.

**Conclusion:** Our results suggest that subsecond MRE of the liver is useful for checking MRE driver settings and monitoring breathing-induced changes in liver stiffness in near real time.

## KEYWORDS

breathing, hepatic perfusion, liver, MRE scout, rapid MR elastography, stiffness

For affiliations refer to page 321

This is an open access article under the terms of the [Creative Commons Attribution-NonCommercial-NoDerivs](https://creativecommons.org/licenses/by-nc-nd/4.0/) License, which permits use and distribution in any medium, provided the original work is properly cited, the use is non-commercial and no modifications or adaptations are made.

© 2023 The Authors. *Magnetic Resonance in Medicine* published by Wiley Periodicals LLC on behalf of International Society for Magnetic Resonance in Medicine.

## 1 | INTRODUCTION

MR elastography (MRE) is a versatile technique that uses changes in tissue stiffness to detect pathologies.<sup>1</sup> Most abdominal applications of MRE focus on the liver because changes in liver tissue can silently progress to a fibrotic state, which is associated with a variety of clinical complications, but are relatively easy to detect by increased tissue stiffness.<sup>2,3</sup>

MRE involves the mechanical generation of shear waves, which are encoded by motion-sensitive phase-contrast MRI sequences.<sup>4</sup> Shear wave excitation requires external hardware and crucially relies on correct driver settings and connections to acoustic energy sources. Direct feedback to the operator is crucial to rule out failure. Furthermore, measured liver stiffness varies during the respiratory cycle<sup>5,6</sup> and with blood perfusion.<sup>7,8</sup> For example, it is recommended to perform MRE in expiration and in a controlled state of fasting,<sup>9–11</sup> and to ask patients to abstain from fluid intake before the examination.<sup>12,13</sup> Today, MRE is considered the most precise method for measuring liver stiffness, outperforming ultrasound elastography.<sup>14</sup> However, unlike elastography by ultrasound, MRE allows only little interaction between the operator and the patient, resulting in limited feedback regarding compliance with breathing instructions or technical issues such as suboptimal wave excitation.<sup>10,15</sup>

Consequently, we identified two major limitations of current abdominal MRE that can potentially be addressed by a rapid MRE technique capable of sampling stiffness maps in the subsecond range: (i) Scout MRE scans for patient-specific adjustment of driver positions and excitation amplitudes prior to more time-consuming MRE protocols involving breath-holds. Using MRE scouts, the operator could easily check shear wave amplitudes—the critical contrast mechanism in MRE—within a region of interest (ROI). (ii) Studies of the effect of breathing on liver stiffness,<sup>16</sup> including assessment of liver physiology and hemodynamics based on stiffness changes, would be greatly facilitated without the need for resynchronizing MRE acquisition to physiological maneuvers. Published studies found liver stiffness measured by rapid ultrasound elastography to be sensitive to the increase in intra-abdominal pressure induced by forced breathing during the Valsalva maneuver.<sup>7,8,17</sup> Previous MRE studies reported significant differences in liver stiffness between inspiration and expiration with higher values during inspiration<sup>18</sup> and increasing differences in patients with fibrosis,<sup>19</sup> motivating the development and use of subsecond MRE for measuring stiffness during free-breathing stiffness measurement.

Here we introduce subsecond rapid MRE of the liver to navigate MRE driver settings and monitor physiological stiffness variations from breathing in near real time.

Single-breath-hold MRE of the liver using simultaneous multislice acquisition<sup>20</sup> has been proposed for 3D MRE, allowing acquisition within 14 to 17 s when combined with fractional encoding<sup>21</sup> and the use of gradient-echo (GRE) sequences.<sup>22</sup> Real-time MRE has been developed using 2D single-shot GRE MRE and stroboscopic wave sampling.<sup>23,24</sup> In stroboscopic wave encoding, a slight mismatch between the TR of the pulse sequence and the oscillation period ensures continuous accumulation of the wave phase, resulting in stiffness mapping at high frame rates on the order of 5 to 6 Hz. However, larger FOV and shorter  $T_2^*$  signal decay times require multishot, segmented acquisitions, precluding stroboscopic sampling in the liver. Therefore, we present a novel MRE concept that sacrifices some of the high temporal resolution of real-time MRE in favor of segmented k-space acquisition for coverage of a large body region, including the liver and adjacent abdominal organs, in arbitrary views in less than a second. We hypothesize that subsecond liver MRE is feasible when performed employing segmented 2D wavefield acquisition with only a few k-space segments and a small number of time steps over a wave period, synchronization of TR to continuous oscillations, and postprocessing that is optimized to reduced wavefield information.

The proposed rapid MRE sequence may offer a useful compromise that, while lacking the volumetric coverage of full 3D MRE, combines the precision of MRE with the rapid feedback on liver stiffness available in ultrasound elastography. To verify our hypothesis, we compare results of our novel MRE sequence with state-of-the-art 3D MRE and ultrasound-based time-harmonic elastography (THE) of the liver.

## 2 | METHODS

Eleven volunteers (8 men; mean age,  $36 \pm 9$  years) without symptoms or a history of liver disease were examined by MRE after written informed consent was obtained. All participants additionally underwent THE on a different day to further investigate breathing-induced stiffness changes observed in MRE.

All subjects were examined in a 3 T MRI scanner (Magnetom Lumina, Siemens Healthineers, Germany) with a 12-channel receiver coil. The abdomen was exposed to vibrations at a frequency of 40 Hz using four custom-made compressed-air drivers attached to the upper trunk with Velcro strips, two on the chest and two on the back. The vibrations were generated with solenoid valves that controlled the airflow by switching them on and off at the desired excitation frequency. To avoid any latency between mechanical stimulation and the time of motion-encoding, the clocks of the vibration generator and the MRI scanner

were synchronized. The resulting modulations in the air-flow were then translated into mechanical deflections by the plastic actuators.<sup>25</sup>

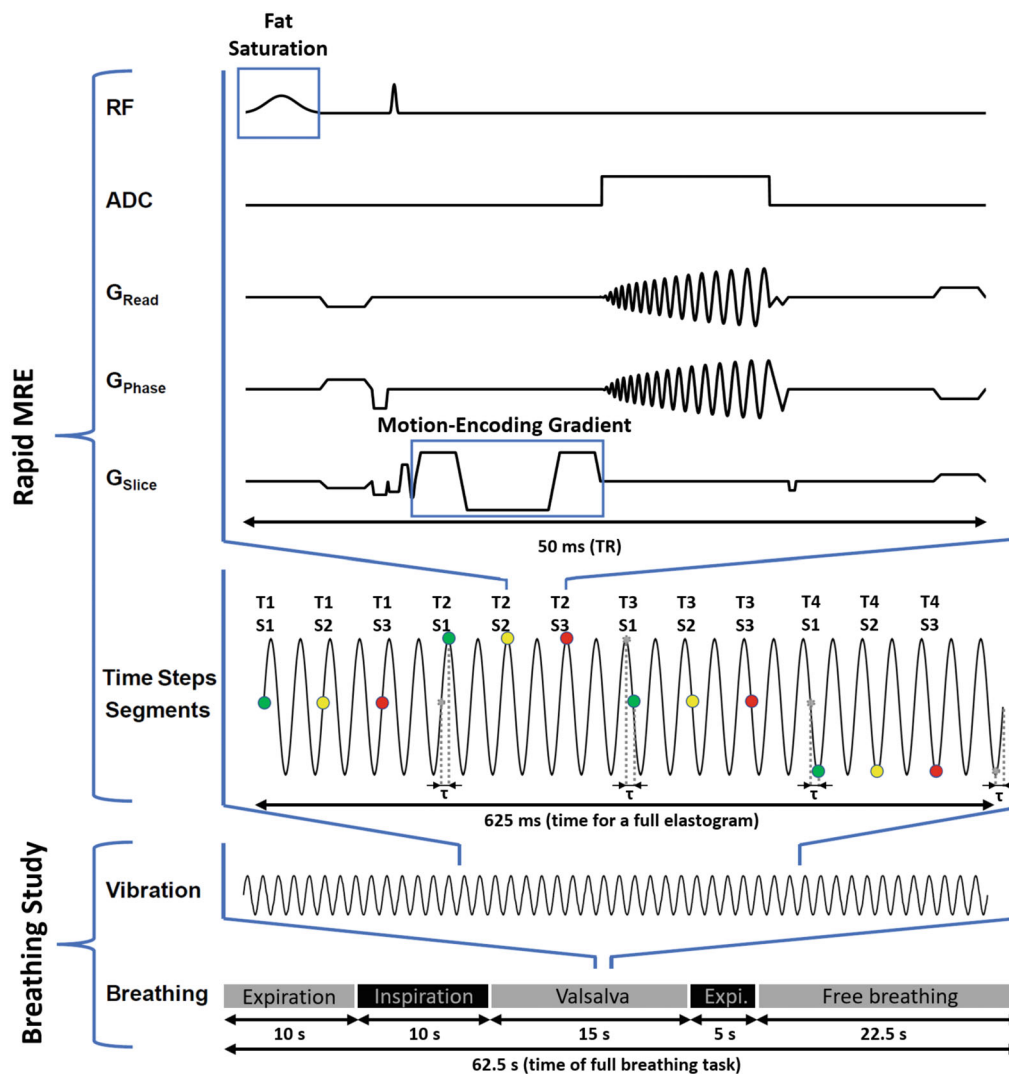
## 2.1 | Sequences

Figure 1 presents the timing diagram of the rapid MRE sequence developed in this study. The sequence had a multishot GRE spiral design sensitized to motion by bipolar motion-encoding gradients (MEGs) with nulled first moments. Each wave image was obtained by interleaving three spiral k-space segments. The spiral trajectory was based on a dual-density design with full sampling in the k-space center and twofold undersampling in the outer area.<sup>26</sup> The repetition time was set to 50 ms, which corresponds to two vibration periods, in order to avoid phase incoherences between the vibration and imaging gradients in different k-space segments. The following imaging parameters were used: FOV = 360 × 360 mm<sup>2</sup>; voxel size = 2.5 × 2.5 × 5.0 mm<sup>3</sup>; single slice; TR = 50 ms; TE = 14 ms; 6/3 (designed/played-out) spiral interleaves; parallel imaging factor of 2 (using iterative self-consistent parallel imaging reconstruction<sup>27</sup> and deblurring based on B<sub>0</sub> field maps<sup>28</sup>); MEG duration = 12.48 ms (nearest possible approximation of 12.5 ms), yielding 28.7 μm/rad encoding efficiency; MEG amplitude = 34 mT/m in thru-plane direction because this component is typically encoded in MRE of the liver.<sup>29</sup> A single stiffness map was generated from four wave images acquired at evenly spaced intervals over a vibration period of 25 ms. For this, after acquisition of a full image, the subsequent acquisition was shifted by 25 ms/4 = 6.25 ms relative to the vibration waveform, resulting in a total acquisition time of 625 ms for a full elastogram ([3 k-space segments × 50 ms TR + 6.25 ms wave-phase shift] × 4 instances over a vibration cycle). Other possible parameter combinations are discussed below.

For comparison, 3D MRE was performed using a Cartesian, single-shot, spin-echo, EPI MRE (SE-EPI-MRE) sequence comprising an asymmetric MEG prior to the refocusing pulse as described in Ref. 30 Image acquisition was performed within a breath-hold using the following parameters: FOV = 360 × 260 mm<sup>2</sup>; 11 slices each of 5 mm thickness; phase partial Fourier = 7/8; 2.5 × 2.5 × 5.0 mm<sup>3</sup> voxel size; 11 slices; TR = 855 ms; TE = 40 ms; parallel imaging factor of 2 (GRAPPA); MEG duration = 12.88 ms (nearest possible approximation of 12.5 ms); MEG amplitude = 34 mT/m; consecutively deployed along all three Cartesian axes, eight instances over a vibration cycle, resulting in a total acquisition time of approximately 21 s for a full 3D elastogram.

## 2.2 | Acquisition protocols

Two MRE experiments were performed in each participant in a single session. First, rapid MRE was performed to check at which air-pressure sufficient wave amplitudes were induced in the liver. Therefore, transverse wave images were acquired to consecutively generate six stiffness maps at different amplitude levels. The input air pressure to the actuators was automatically increased from 0 mbar to 1000 mbar in 200 mbar increments with 2 s forerun time to reach a mechanical steady state. Overall, this scout experiment took a total scan time of  $6 \times (2 + 0.625) = 15.75$  s, during which each participant was asked to hold their breath in end-expiration, which is the recommended breathing state in liver MRE.<sup>10</sup> For comparison with established 3D MRE, the SE-EPI-MRE sequence was applied in the same transverse orientation as the rapid MRE 2D-slice. SE-EPI-MRE acquisition was performed during both end-expiratory and end-inspiratory breath-holds without moving the position of the 3D slice block to test possible effects of different breath-hold states on liver stiffness. Because the position of the liver varied significantly between the two breath-hold positions, we selected different slices from the 3D blocks that matched the anatomy of the liver depicted by the 2D rapid MRE sequence. In a second experiment, we used the optimized pressure settings from the first experiment and studied the respiration-induced shift in liver position along the feet-head direction using a coronal view. Here, a series of 100 MRE maps were acquired continuously over 62.5 s to capture the dynamic changes in liver stiffness induced by different breathing patterns and maneuvers. The coronal view allowed us to correct for feet-head motion of the liver using image registration for improved comparison. Each participant performed a sequence of five different breathing maneuvers following the instructions given by the operator via the MRI communication system. The sequence of breathing maneuvers is illustrated in Figure 1. First, the participants were asked to exhale and maintain the state of end-expiratory breath-hold for 10 s, followed by fast inhalation and an end-inspiration breath-hold for another 10 s. The acquisition was then continued without breathing but increased abdominal pressure through the Valsalva maneuver for 15 s, followed by a short phase of expiration for 5 s and free breathing during the remaining 22.5 s. Prior to the experiments, the participants were trained in this respiratory protocol, including the Valsalva maneuver, by ventilating against a manometer to ensure that an abdominal pressure corresponding to approximately 50 mbar expiration pressure was maintained during the scan.



**FIGURE 1** Rapid MRE sequence and timing relative to external vibration of 40 Hz and respiration. Each elastogram was generated from wave data encoded at four different time points over a vibration period (T1–T4) using a segmented spiral gradient-echo sequence with three interleaved spiral readouts as demarcated by green, yellow, and red circles (S1–S3). After acquisition of these three k-space segments, each of which had a TR of 50 ms corresponding to two vibration cycles, the start of the subsequent image acquisition was shifted by  $\tau = 6.25$  ms, indicated by the displacement of the gray points toward the green points. Consequently, after four images, a full vibration cycle was encoded, resulting in a total acquisition time of 625 ms for a full elastogram. In a second experiment with time-resolved rapid MRE sequence, 100 elastograms were continuously acquired over 62.5 s in order to capture breathing-induced changes in stiffness. The breathing paradigm consisted of five consecutive maneuvers of expiration breath-hold (10 s), inspiration breath-hold (10 s), Valsalva maneuver (15 s), expiration breath-hold (5 s), and free breathing for the remaining acquisition. ADC, analog-to-digital converter; MRE, MR elastography.

### 2.3 | Time-harmonic elastography

THE of the liver was performed, as described in Ref. 8, once during an end-inspiratory breath-hold and once during an end-expiratory breath-hold. In brief, the subjects were positioned supine on a bed with an integrated vibration generator. A multifrequency waveform of six frequencies (27, 33, 39, 44, 50, 56 Hz) was used for continuous mechanical excitation. Anatomy and motion were detected by a

commercial elastography system (GAMPT mbH, Merseburg, Germany) using a curved-array C5-H2 transducer at 2 MHz. For acquisition, the transducer was positioned in the left intercostal space to image the right liver lobe. Data were acquired at a depth of 120 mm and an 80 Hz frame rate over 1 s. Stiffness maps were generated using the same algorithm as for MRE.<sup>31</sup> Note that, because the liver moves out of the imaging during respiration, continuous acquisition of hepatic elastograms by THE is not possible.



## 2.4 | Data postprocessing

Stiffness maps in terms of shear wave speed (SWS, in m/s) were reconstructed by wavenumber ( $k$ )-based multifrequency dual elasto-visco inversion method, as proposed in 2016 by Tzschäetzsch et al.<sup>31</sup> and recently made available on a publicly accessible server by Meyer et al.<sup>32</sup> Because our novel MRE technique acquires less information than standard multicomponent and multifrequency MRE, the smoothing capacity of the pipeline was slightly increased by using a third-order Butterworth high-pass filter with a 94 rad/m threshold instead of the conventional linear high-pass filter.<sup>32</sup> Furthermore, the directional filters with Gaussian kernels (eight spatial directions) were replaced by cosine-squared kernels (four directions). Motion correction was performed in all coronal images based on spatial normalization<sup>33</sup> to align the liver position in the 2D image slice with the ROI of the entire liver manually selected from the image acquired at the first time point. This image was used as reference for registration of the liver in serial coronal images. Therefore, in-plane rigid body motion correction was applied to the complex MRI data prior to MRE postprocessing as described in Shahyari et al.<sup>6</sup>

## 2.5 | Statistics

Mean values were obtained from manually selected ROIs covering the full liver visible within the 2D slices. Bonferroni-corrected paired Wilcoxon tests with a level of significance of 0.05 were used for all comparisons of group mean SWS values. Wave amplitudes and SNRs were computed from the magnitudes of complex-valued shear wave fields and wavelet-based noise analysis of the displacement fields, respectively.<sup>34</sup> A one-way repeated measures analysis of variance test with Bonferroni correction was performed to investigate the effect of different pressure levels on the SD of SWS and SNR. Optimal thresholds for wave amplitude and displacement SNR to exclude too noisy shear waves were derived by histogram analysis of pixel values in the livers of all subjects.

## 3 | RESULTS

SWS maps in a transverse view of a representative volunteer are shown in Figure 2A, demonstrating that rapid MRE can be used to quickly assess whether generated waves fully penetrate the liver before more

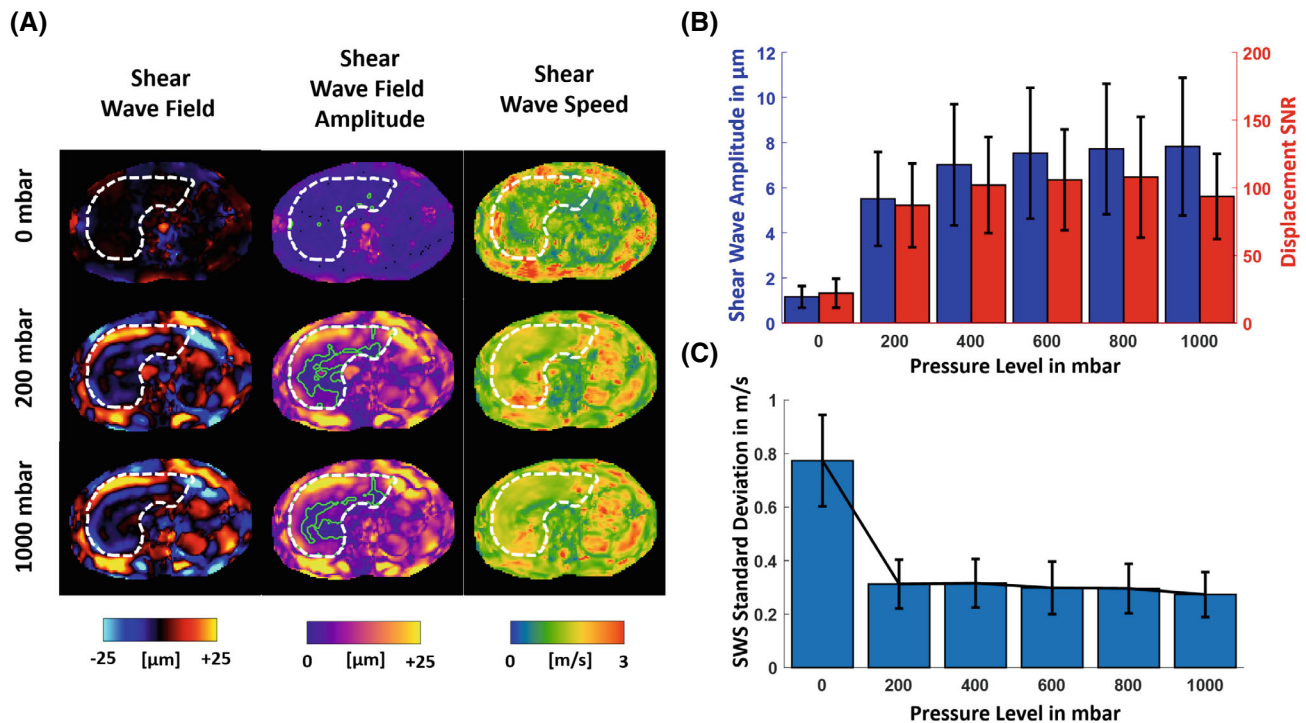


**FIGURE 2** Shear wave fields and shear wave speed maps in a transverse view through the abdomen acquired with the rapid MRE sequence within 625 ms. (A) Real part of the complex-valued shear wave field, amplitude of the shear wave field, and shear wave speed shown in the left, middle, and right column, respectively, at different pressure levels of the actuators. White dashed lines demarcate the liver region; green lines indicate the regions inside the liver which were automatically detected as being reliable for stiffness measurement based on wave amplitude thresholds ( $>3.6 \mu\text{m}$ ). (B) Shear wave amplitudes and displacement SNR within the liver at increasing drive pressure from 0 to 1000 mbar. (C) SD of shear wave speed within the liver at increasing drive pressure from 0 to 1000 mbar.

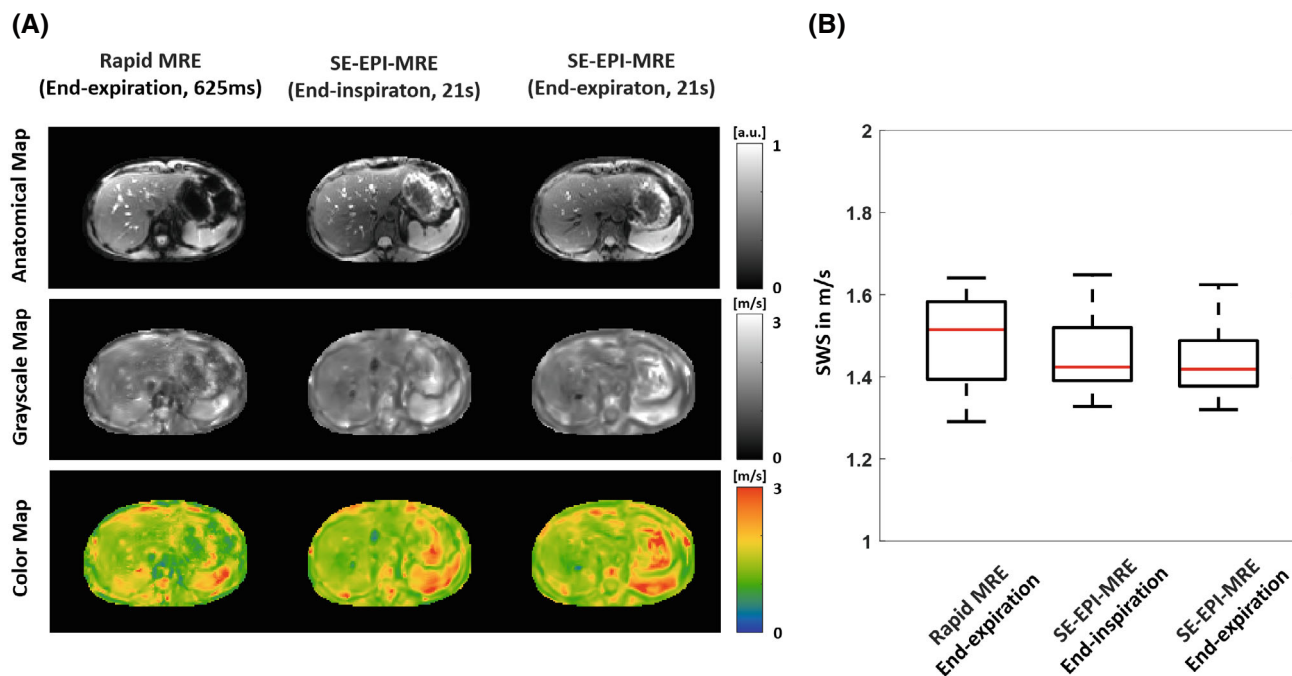


**FIGURE 3** SWS obtained by rapid MRE and SE-EPI-MRE. (A) Representative anatomical images (MRE magnitude signal) and SWS maps obtained with the two sequences. Whereas SE-EPI-MRE covered a full volume in which similar slices were identified in end-expiration and end-inspiration, the rapid MRE sequence captured only a single slice in end-expiration to avoid tissue displacement due to respiration. Despite notable differences in image position and organ morphology due to respiration, both sequences provide similar detail resolution. (B) Group statistical plots of mean SWS of liver tissue visible in the slices shown in (A). SE-EPI-MRE, spin-echo, echo-planar-imaging MRE; SWS, shear wave speed.

time-consuming examinations are performed. Figure 2B shows the increase in wave amplitudes in the livers of all subjects as the air pressure applied to the actuators increased. Shear wave amplitudes increased from  $1.16 \pm 0.48 \mu\text{m}$  at 0 mbar (indicating noise) to  $7.82 \pm 3.06 \mu\text{m}$  at 1000 mbar (full deflection amplitudes,  $p < 0.0001$ ), whereas there was no notable change for drive pressures exceeding 600 mbar ( $p > 0.05$ ). For wave amplitudes between 0 mbar (noise) and 200 mbar (significant amplitudes), we found an optimal threshold of  $3.6 \mu\text{m}$  (indicated by green lines in Figure 2A). Similar to wave amplitudes, displacement SNR increased from  $22.12 \pm 10.75$  to  $93.56 \pm 31.45$  ( $p < 0.001$ ), with an optimal SNR threshold of 38.18 to exclude noisy wave amplitudes in all livers from analysis. SD of liver SWS is shown in Figure 2C. Note the steep decrease from  $0.77 \pm 0.17 \text{ m/s}$  to  $0.31 \pm 0.09 \text{ m/s}$  at 0 and 200 mbar, respectively ( $p < 0.001$ ). Again, an optimal threshold, namely an SWS SD of 0.55, ensured sufficient wave amplitudes already at 200 mbar vibration pressure. Eight of 11 subjects found the vibration amplitudes at 1000 mbar still acceptable, whereas three described them to be slightly uncomfortable. All subjects reported the vibration amplitudes at 200 mbar to be negligible. Therefore, 200 mbar was the drive pressure recommended for the experiments described below.

Figure 3 compares the results and quality of the SWS maps obtained by 2D rapid MRE and 3D SE-EPI-MRE for the same volunteer. Similar transverse slices are shown for end-inspiration and end-expiration selected from the same 3D MRE scan and corresponding to the 2D MRE slice that was acquired during end-expiration. It should be noted that the transverse 2D rapid MRE scan was only acquired during end-expiratory breath-hold to avoid readjustment of the slice position that would have been necessary due to liver movement. Grayscale and color maps are displayed because quantitative values are better captured by color maps, whereas details are better seen in grayscale maps. Overall, image quality and detail resolution of SWS maps were similar for the two methods. Note that our novel MRE sequence acquired only four wave dynamics and one wave component, whereas 3D MRE maps were reconstructed from eight wave dynamics and three field components. Quantitative SWS values of the liver were similar in all three images as demonstrated in Figure 3B, with slightly higher percentile ranges in rapid MRE than 3D MRE. Mean liver SWS values were  $1.48 \pm 0.12 \text{ m/s}$ ,  $1.46 \pm 0.10 \text{ m/s}$ , and  $1.43 \pm 0.09 \text{ m/s}$  for rapid MRE, 3D MRE (end-inspiration), and 3D MRE (end-expiration), respectively, without significant differences.

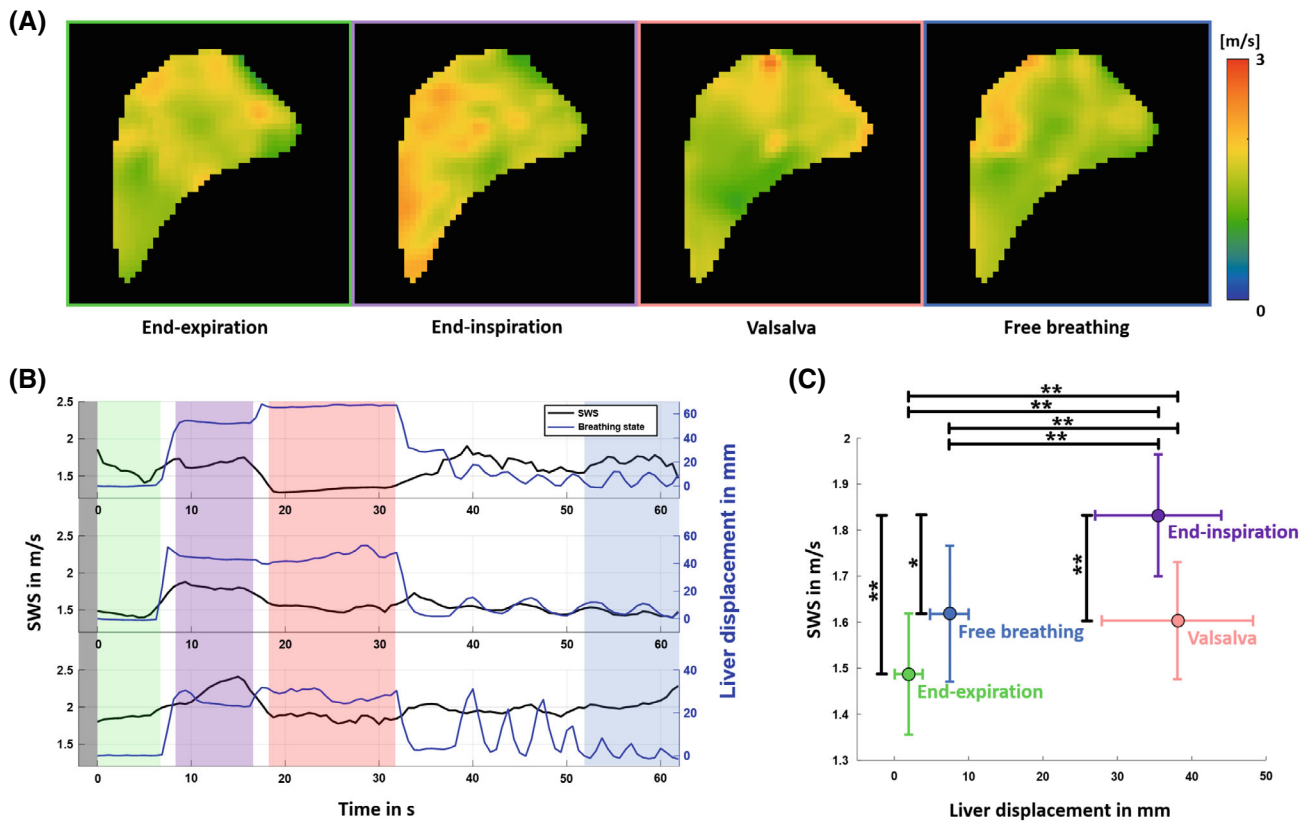


**FIGURE 4** Use of rapid MRE for time-resolved measurement of liver stiffness during breathing in a coronal view. (A) Representative SWS maps corresponding to the defined breathing states after motion correction using image registration. Color-coded frames indicate precise breathing states (green: end-expiration breath-hold; purple: end-inspiration breath-hold; red: Valsalva; blue: free breathing). All 100 SWS maps acquired within 62.5 s are provided as supplemental Figure S1. (B) SWS and displacement data obtained from image registration averaged within the liver for three volunteers (the upper row corresponds to the subject shown in (A)). The colors demarcate the phases of breathing within which SWS was averaged for group analysis. The gray phase (2 s) represents the transition period before tissue oscillation reaches equilibrium. (C) Group statistical plot of means and 95% confidence intervals for SWS and liver displacement during different breathing maneuvers. \* $p < 0.05$ , \*\* $p < 0.01$ .

The use of our novel MRE sequence to study the influence of breathing on SWS is illustrated in Figure 4. Representative SWS maps after image registration for breathing motion correction show the pixel-wise changes in SWS during different breathing maneuvers. The full series of 100 coronal SWS maps is available as Supporting Information (see Figure S1). Overall liver stiffness in the volunteer shown was apparently higher at end-inspiration compared to both the Valsalva maneuver ( $p < 0.01$ ) and end-expiration ( $p < 0.01$ ). Movies of SWS maps covering all breathing maneuvers investigated in one of the volunteers, with and without image registration, are provided as Video S1. The time courses of spatial means shown in Figure 4B for three volunteers corroborate our visual interpretation of the SWS maps presented in Figure 4A. Moreover, displacement curves obtained from image registration are plotted, indicating the breathing-induced physiological displacement of the liver along the feet-head direction. Remarkably stable

SWS values were obtained despite pronounced motion patterns during the free-breathing phase following the Valsalva maneuver. Shear wave amplitudes also did not significantly vary with breathing. Group mean SWS values and liver displacements for the phases in all 11 subjects are shown in Figure 4C for the four color-coded phases in Figure 4A,B. The lowest SWS values were observed during end-expiration ( $1.49 \pm 0.22$  m/s), but the values were not significantly different from those obtained during the Valsalva maneuver ( $1.60 \pm 0.22$  m/s) and free breathing ( $1.62 \pm 0.25$  m/s), again suggesting that end-expiration is the best controlled breathing state for liver MRE. However, a significant difference was observed between SWS at end-expiration and peak SWS at end-inspiration ( $1.83 \pm 0.22$  m/s,  $p < 0.01$ ). This reproduced the main finding of higher SWS values after inspiration ( $1.36 \pm 0.06$  m/s) than expiration ( $1.30 \pm 0.06$  m/s,  $p < 0.05$ ) while providing lower values than MRE ( $p < 0.01$ ), as discussed below. No change in wave amplitudes was induced by the different

breathing maneuvers (all  $p > 0.05$ ). All SWS values are summarized in Table 1. Our results for liver displacement, shear wave amplitudes, and SWS values for the four respiratory states investigated are summarized in Table S1.

## 4 | DISCUSSION

Here, we present a novel MRE sequence based on a multishot, GRE sequence with spiral readout. With an acquisition time of 625 ms for obtaining 2D SWS maps of the abdomen, this, to our knowledge, is the fastest MRE method available for liver studies to date. As shown by the two experiments we conducted, the method can be used to optimize parameter settings and to assess elastogram quality before acquiring higher-dimensional MRE. It can also be used to study potential changes in stiffness related to physiological changes in geometry, blood flow, or abdominal pressures that can be induced in the liver by breathing.

Our sequence provides a technical solution for short  $T_2^*$  relaxation times in larger FOVs, where organs, such as the liver, can move and deform moderately during the respiratory cycle. The key innovation is based on 2D k-space sampling with only a few segments (three), time steps (four), and wave components (one), and TR adaptation to multiple integer periods (2 of 40 Hz) of externally induced continuous oscillations (requiring clock synchronization between wave generator and MRI scanner). These specific parameters that we used here could be further optimized for higher frequencies, shorter TR, and fewer time points in the vibration cycle. For example, retaining 3 k-space segments and shortening the MEG to 11.5 ms would allow TR to be reduced to 40 ms, which could be matched to two oscillation periods of 50 Hz. Furthermore, reducing the number of time steps to three would result in even shorter sampling times of  $9 \cdot 40 + 20 \text{ ms} = 380 \text{ ms}$ , provided that image quality is sufficient for MRE inversion. This demonstrates the generalizability of our technique to further optimize rapid MRE sequences.

The potential benefit of rapid MRE scout scans to obtain information on whether shear waves penetrate the ROI has been discussed in the literature.<sup>4</sup> Involving external hardware, MRE is susceptible to technical failure if adequate feedback on the operational status of the equipment is not available. For example, inadequate placement of actuators or failure of acoustic power transmission could diminish wave amplitudes, degrading stiffness maps or even corrupting the entire examination. A rapid MRE scan can quickly provide feedback, so the operator can check for potential deficiency of shear waves or adjust driver positions and wave amplitudes prior to the actual clinical MRE scan of interest. Moreover, patient awareness

of MRE actuator vibrations, combined with the feedback received by the operator, could further increase the success rate of clinical MRE<sup>35–37</sup> and minimize technical failures related to mechanical excitation at low costs.

In our experiments, we demonstrated the consistency of SWS values obtained by our novel MRE sequence in comparison with SE-EPI-MRE, which has become an established MRE technique for the liver.<sup>25,38,39</sup> SE-EPI-MRE is more susceptible to off-resonance-related distortion artifact than segmented spiral readout sequences,<sup>40,41</sup> whereas the latter are more susceptible to blurring artifacts. Other k-space sampling schemes for fast GRE MRE, such as radial readout, have been proposed and are currently being tested.<sup>42</sup> The fact that SE-EPI-MRE could not resolve a difference in stiffness between the end of inspiration and end of expiration may be attributable to the long scan time and breath-hold phases (21 s vs. 10 s in our breathing experiment) (Figure 4), which averages out temporal effects. Because THE is a rapid method for stiffness measurement (1 s acquisition time), it has been used as a robust tool to test physiologic effects in elastography.<sup>43</sup> However, in this study, THE identified only a slight difference in stiffness between end-inspiration and end-expiration (5%), whereas rapid MRE detected a much larger effect of nearly 24%. We believe that rapid MRE in the coronal view captures the instantaneous response of liver stiffness to respiration better than THE because, during an ultrasound examination, the operator must readjust the probe position and acoustic window after each breathing command. This also indicates that the timing of the maneuver is more important than the net duration of data acquisition. It is worthwhile to mention that THE provided slightly lower values than MRE (approximately 1.3 m/s vs. 1.5 m/s). This is possibly due to the high SWS dispersion of healthy liver, which may shift the effective center frequency of the multifrequency shear waves from 41.5 Hz to lower values, thus reducing the measured effective SWS.<sup>44</sup>

A rich body of literature reports MRE of the liver under various conditions of blood perfusion, fasting, and breathing. A marked postprandial increase in liver stiffness has been observed in both patients with chronic liver disease<sup>45</sup> and healthy volunteers<sup>11</sup> and has been shown to correlate with portal venous flow.<sup>46</sup> These findings have led to the recommendation that MRE should be performed in a controlled fasted state.<sup>9</sup> Furthermore, MRE is typically performed at end-expiration<sup>10</sup> because the state of breathing during the MRE scan was identified as a confounder of liver stiffness.<sup>18,19</sup> Both breathing and eating affect hepatic perfusion, suggesting that enhanced hemodynamic activity of the liver and the resulting higher intravascular pressure are associated with increased tissue stiffness. This notion was supported by the observation



TABLE 1 Mean values and SDs of shear wave speed within the liver for each subject and group values acquired in different experiments of this study

No.	Rapid MRE study				Breathing study				Ultrasound elastography				
	SE-EPI-MRE	SE-EPI-MRE	Rapid MRE	Rapid MRE	Rapid MRE	Rapid MRE	Rapid MRE	Rapid MRE	Rapid MRE	Free breathing	THE	THE	THE
	Breath hold state												
	End-Expiration	End-Inspiration	End-Expiration	End-Expiration	End-Expiration	End-Inspiration	End-Inspiration	Valsalva	Free breathing	End-Expiration	End-Inspiration		
	Mean and SD of SWS Values in m/s												
1	1.45 ± 0.38	1.51 ± 0.18	1.37 ± 0.18	1.22 ± 0.06	1.89 ± 0.30	1.67 ± 0.07	1.34 ± 0.02	1.25 ± 0.02	1.30 ± 0.02				
2	1.52 ± 0.17	1.39 ± 0.17	1.38 ± 0.22	1.90 ± 0.17	2.27 ± 0.22	1.86 ± 0.21	2.05 ± 0.26	1.23 ± 0.02	1.33 ± 0.07				
3	1.60 ± 0.31	1.60 ± 0.22	1.52 ± 0.19	1.31 ± 0.03	1.54 ± 0.22	1.33 ± 0.10	1.41 ± 0.10	1.37 ± 0.04	1.52 ± 0.05				
4	1.61 ± 0.38	1.38 ± 0.24	1.42 ± 0.18	1.39 ± 0.07	1.58 ± 0.09	1.37 ± 0.09	1.46 ± 0.06	1.26 ± 0.03	1.30 ± 0.03				
5	1.51 ± 0.13	1.46 ± 0.22	1.44 ± 0.18	1.51 ± 0.08	1.80 ± 0.22	1.54 ± 0.11	1.45 ± 0.06	1.35 ± 0.04	1.38 ± 0.06				
6	1.29 ± 0.18	1.33 ± 0.16	1.32 ± 0.15	1.22 ± 0.06	1.68 ± 0.06	1.55 ± 0.04	1.65 ± 0.08	1.38 ± 0.04	1.37 ± 0.02				
7	1.32 ± 0.43	1.41 ± 0.18	1.38 ± 0.19	1.59 ± 0.21	1.68 ± 0.06	1.32 ± 0.06	1.68 ± 0.24	1.23 ± 0.03	1.29 ± 0.03				
8	1.50 ± 0.32	1.52 ± 0.25	1.50 ± 0.22	1.45 ± 0.04	1.86 ± 0.31	1.56 ± 0.10	1.61 ± 0.04	1.39 ± 0.03	1.35 ± 0.04				
9	1.64 ± 0.38	1.65 ± 0.23	1.62 ± 0.27	1.84 ± 0.25	2.14 ± 0.23	1.92 ± 0.27	2.14 ± 0.24	1.28 ± 0.06	1.40 ± 0.04				
10	1.37 ± 0.24	1.42 ± 0.19	1.42 ± 0.18	1.48 ± 0.06	1.94 ± 0.34	1.87 ± 0.08	1.40 ± 0.05	1.25 ± 0.04	1.33 ± 0.02				
11	1.52 ± 0.36	1.40 ± 0.19	1.38 ± 0.18	1.45 ± 0.04	1.78 ± 0.14	1.66 ± 0.08	1.52 ± 0.04	1.36 ± 0.04	1.36 ± 0.07				
Group	1.48 ± 0.12	1.46 ± 0.10	1.43 ± 0.09	1.49 ± 0.22	1.83 ± 0.22	1.60 ± 0.22	1.62 ± 0.25	1.30 ± 0.06	1.36 ± 0.06				

Abbreviations: MRE, MR elastography; SE-EPI-MRE, spin-echo, echo-planar-imaging MRE; SWS, shear wave speed; THE, time-harmonic elastography.

that liver stiffness was higher after ingestion of water,<sup>12,13</sup> whereas relief of high portal pressure by shunting was reported to cause a decrease in stiffness.<sup>47,48</sup> Furthermore, a higher intra-abdominal pressure as generated by the Valsalva maneuver can lead to a collapse of hepatic veins and overall reduction of liver perfusion, resulting in hepatic softening.<sup>7,8</sup> Conversely and in agreement with previous studies,<sup>18,19</sup> our results at end-inspiration suggest that preserved hepatic flow in the presence of elevated intra-abdominal pressure leads to higher stiffness values. Although these results provide strong evidence for hepatohemodynamic effects on tissue stiffness, they are correlative and not causal. Beyond blood perfusion, other factors such as geometric deformation with compression stiffening<sup>49</sup> or changes in the metabolic state of hepatocytes might dynamically alter liver stiffness.<sup>50</sup> In any case, by measuring dynamic changes in tissue stiffness, the proposed rapid MRE sequence could open a window into the study of relationships between biomechanics and function/perfusion properties of abdominal tissues, similar to what has recently been reported for other tissues and organs such as the lower extremities<sup>23</sup> or the brain.<sup>24</sup>

Our study has limitations. First, by nature of the design as an exploratory, technical feasibility study, only healthy participants were investigated. It would be interesting to test a short clinical protocol in patients with chronic liver diseases and detect possible stiffness differences between inspiration and expiration within approximately two breathing cycles. Such dynamic property changes might reveal the alteration of the dynamic component of liver stiffness better than two static measurements.<sup>19</sup> A technical limitation is the restriction of our novel MRE technique to 2D, whereas shear waves in the abdomen are 3D vector fields. Therefore, a geometric bias may occur if the slices are not optimally aligned with respect to the wave propagation direction. However, the k-based multi-inversion method that we used mitigates the geometric bias by incorporating spatiotemporal filters that favor in-plane propagating waves while suppressing waves that cross the image plane obliquely. In addition, the cosine dependence of the geometric bias, as discussed in Ref. 51 minimizes the effect of oblique waves on the resulting 2D SWS maps. A further technical limitation is that we did not implement the data processing pipeline on our MRI scanner; thus, rapid MRE images were computed offline, and the wave amplitude information and stiffness maps were not available to us until after the examinations. However, as mentioned earlier, the goal of this study was to demonstrate the technical feasibility of our novel MRE technique and its use for rapid measurement of liver stiffness during the respiratory cycle. After this successful pilot study, we plan to fully implement the postprocessing pipeline of rapid MRE on our MRI system. Once phase

images have been received from the MRI system's computer, MRE inversion can be performed within a fraction of a second.

## 5 | CONCLUSION

This study shows the feasibility of rapid MRE for subsecond sampling of abdominal stiffness. The viable method can be used for navigating the setup of MRE driver hardware and postprocessing pipelines as well as for detecting stiffness variations due to breathing-induced changes in abdominal pressure and blood flow to the liver. Using rapid MRE for quantification of liver stiffness changes attributable to breathing, we observed a decrease in stiffness from end-inspiration, to Valsalva maneuver, to end-expiration. Overall, with the findings presented here, this approach has opened the door to instantaneous measurement of tissue stiffness in abdominal organs using MRE, with quasi real-time resolution similar to ultrasound elastography but less limited in terms of image positioning and data quality, and the possibility of using the scan as a scout for externally induced shear waves.

## AFFILIATIONS

<sup>1</sup> Department of Radiology, Charité—Universitätsmedizin Berlin, Corporate Member of Freie Universität Berlin and Humboldt-Universität zu Berlin, Berlin, Germany

<sup>2</sup> Application Development, Siemens Healthcare GmbH, Erlangen, Germany

<sup>3</sup> Berlin Center for Advanced Neuroimaging (BCAN), Berlin, Germany, Corporate Member of Freie Universität Berlin, Berlin Institute of Health and Humboldt-Universität zu Berlin, Berlin, Germany

<sup>4</sup> Physikalisch-Technische Bundesanstalt (PTB), Braunschweig and Berlin, Berlin, Germany

<sup>5</sup> Department of Medical Physics, University of Wisconsin, Madison, Wisconsin USA

<sup>6</sup> Department of Radiology, University of Wisconsin, Madison, Wisconsin USA

<sup>7</sup> Charité—Universitätsmedizin Berlin, Corporate Member of Freie Universität Berlin and Humboldt-Universität zu Berlin, Berlin, Germany

<sup>8</sup> Working Group On CMR, Experimental and Clinical Research Center, a cooperation between the Max Delbrück Center for Molecular Medicine in the Helmholtz Association and the Charité—Universitätsmedizin Berlin, Berlin, Germany

<sup>9</sup> DZHK (German Centre for Cardiovascular Research), partner site Berlin, Berlin, Germany

<sup>10</sup> Department of Cardiology and Nephrology, HELIOS Hospital Berlin-Buch, Berlin, Germany

<sup>11</sup> Department of Medical Engineering, Technische Universität Berlin, Einstein Centre Digital Future, Berlin, Germany

<sup>12</sup> Institute of Medical Informatics, Charité—Universitätsmedizin Berlin, Corporate Member of Freie Universität Berlin and Humboldt-Universität zu Berlin, Berlin, Germany

## ACKNOWLEDGMENTS

We thank the German Research Foundation (DFG) for funding (RTG2260 BIOQIC, CRC1340 Matrix-in-vision). Open Access funding enabled and organized by Projekt DEAL.

## ORCID

Matthias Anders  <https://orcid.org/0000-0002-6447-2029>

Tom Meyer  <https://orcid.org/0000-0002-2171-6791>

Carsten Warmuth  <https://orcid.org/0000-0001-8785-1999>

Josef Pfeuffer  <https://orcid.org/0000-0001-9887-0458>

Heiko Tzschätzsch  <https://orcid.org/0000-0001-9458-2221>

Helge Herthum  <https://orcid.org/0000-0001-6494-0833>

Mehrgan Shahryari  <https://orcid.org/0000-0002-3981-1711>

Katja Degenhardt  <https://orcid.org/0000-0002-0482-9698>

Oliver Wieben  <https://orcid.org/0000-0002-7931-1930>

Sebastian Schmitter  <https://orcid.org/0000-0003-4410-6790>


Jeanette Schulz-Menger  <https://orcid.org/0000-0003-3100-1092>

Tobias Schaeffter  <https://orcid.org/0000-0003-1310-2631>

Juergen Braun  <https://orcid.org/0000-0001-5183-7546>

Ingolf Sack  <https://orcid.org/0000-0003-2460-1444>

## TWITTER

Ingolf Sack  [@bioqic@twitter.de](https://twitter.com/bioqic)

## REFERENCES

- Muthupillai R, Lomas D, Rossman P, Greenleaf JF, Manduca A, Ehman RL. Magnetic resonance elastography by direct visualization of propagating acoustic strain waves. *Science*. 1995;269:1854-1857.
- Garteiser P, Doblaz S, Van Beers BE. Magnetic resonance elastography of liver and spleen: methods and applications. *NMR Biomed*. 2018;31:3891.
- Idilman IS, Li J, Yin M, Venkatesh SK. MR elastography of liver: current status and future perspectives. *Abdom Radiol*. 2020;45:3444-3462.
- Sack I. Magnetic resonance elastography from fundamental soft-tissue mechanics to diagnostic imaging. *Nat Rev Phys*. 2023;5:25-42.
- Murphy IG, Graves MJ, Reid S, et al. Comparison of breath-hold, respiratory navigated and free-breathing MR elastography of the liver. *Magn Reson Imaging*. 2017;37:46-50.
- Shahryari M, Meyer T, Warmuth C, et al. Reduction of breathing artifacts in multifrequency magnetic resonance elastography of the abdomen. *Magn Reson Med*. 2021;85:1962-1973.
- Ipek-Ugay S, Tzschätzsch H, Braun J, Fischer T, Sack I. Physiologic reduction of hepatic venous blood flow by the Valsalva maneuver decreases liver stiffness. *J Ultrasound Med*. 2017;36:1305-1311.
- Meyer T, Tzschätzsch H, Wellge B, Sack I, Kröncke T, Martl A. Valsalva maneuver decreases liver and spleen stiffness measured by time-harmonic ultrasound elastography. *Front Bioeng Biotechnol*. 2022;10:886363.
- Manduca A, Bayly PV, Ehman RL, et al. MR elastography: principles, guidelines, and terminology. *Magn Reson Med*. 2021;85:2377-2390.
- Guglielmo FF, Venkatesh SK, Mitchell DG. Liver MR elastography technique and image interpretation: pearls and pitfalls. *Radiographics*. 2019;39:1983-2002.
- Obrzut M, Atamaniuk V, Chen J, et al. Postprandial hepatic stiffness changes on magnetic resonance elastography in healthy volunteers. *Sci Rep*. 2021;11:19786.
- Ipek-Ugay S, Tzschätzsch H, Hudert C, et al. Time harmonic elastography reveals sensitivity of liver stiffness to water ingestion. *Ultrasound Med Biol*. 2016;42:1289-1294.
- Dittmann F, Tzschätzsch H, Hirsch S, et al. Tomoelastography of the abdomen: tissue mechanical properties of the liver, spleen, kidney, and pancreas from single MR elastography scans at different hydration states. *Magn Reson Med*. 2017;78:976-983.
- Horowitz JM, Kamel IR, Arif-Tiwari H, et al. ACR appropriateness criteria<sup>®</sup> chronic liver disease. *J Am Coll Radiol*. 2017;14:391-405.
- Hudert CA, Tzschätzsch H, Rudolph B, et al. How histopathologic changes in pediatric nonalcoholic fatty liver disease influence in vivo liver stiffness. *Acta Biomater*. 2021;123:178-186.
- Mueller S. *Liver Elastography. Clinical Use and Interpretation*. Springer; 2020.
- Millonig G, Friedrich S, Adolf S, et al. Liver stiffness is directly influenced by central venous pressure. *J Hepatol*. 2010;52:206-210.
- Wang K, Manning P, Szeverenyi N, et al. Repeatability and reproducibility of 2D and 3D hepatic MR elastography with rigid and flexible drivers at end-expiration and end-inspiration in healthy volunteers. *Abdom Radiol*. 2017;42:2843-2854.
- Ren H, Yang D, Xu H, et al. Effect of breath holding at the end of the inspiration and expiration phases on liver stiffness measured by 2D-MR elastography. *Abdom Radiol*. 2021;46:2516-2526.
- Majeed W, Kalra P, Kolipaka A. Simultaneous multislice rapid magnetic resonance elastography of the liver. *NMR Biomed*. 2020;33:e4252.
- Klatt D, Asbach P, Rump J, et al. In vivo determination of hepatic stiffness using steady-state free precession magnetic resonance elastography. *Invest Radiol*. 2006;41:841-848.
- Guenther C, Sethi S, Troelstra M, Dokumaci AS, Sinkus R, Kozerke S. Ristretto MRE: a generalized multi-shot GRE-MRE sequence. *NMR in Biomed*. 2019;32:4049.
- Schrank F, Warmuth C, Görner S, et al. Real-time MR elastography for viscoelasticity quantification in skeletal muscle during dynamic exercises. *Magn Reson Med*. 2020;84:103-114.
- Herthum H, Shahryari M, Tzschätzsch H, et al. Real-time multifrequency MR elastography of the human brain reveals rapid changes in viscoelasticity in response to the Valsalva maneuver. *Front Bioeng Biotechnol*. 2021;9:666456.

25. Shahryari M, Tzschätzsch H, Guo J, et al. Tomoelastography distinguishes non-invasively between benign and malignant liver lesions. *Cancer Res.* 2019;79:5704-5710.
26. Meyer CH, Zhao L, Lustig M, et al. Dual-density and parallel spiral ASL for motion artifact reduction. In Proceedings of the 19th Annual Meeting of ISMRM, Montréal, Québec, Canada, 2011. p 3986.
27. Lustig M, Pauly JM. SPIRiT: iterative self-consistent parallel imaging reconstruction from arbitrary k-space. *Magn Reson Med.* 2010;64:457-471.
28. King KF, Ganin A, Zhou XJ, Bernstein MA. Concomitant gradient field effects in spiral scans. *Magn Reson Med.* 1999;41:103-112.
29. Venkatesh SK, Yin M, Ehman RL. Magnetic resonance elastography of liver: technique, analysis, and clinical applications. *J Magn Reson Imaging.* 2013;37:544-555.
30. Dittmann F, Hirsch S, Tzschätzsch H, Guo J, Braun J, Sack I. In vivo wideband multifrequency MR elastography of the human brain and liver. *Magn Reson Med.* 2016;76:1116-1126.
31. Tzschätzsch H, Trong MN, Scheuermann T, et al. Two-dimensional time-harmonic elastography of the human liver and spleen. *Ultrasound Med Biol.* 2016;42:2562-2571.
32. Meyer T, Marticorena Garcia S, Tzschätzsch H, et al. Comparison of inversion methods in MR elastography: an open-access pipeline for processing multifrequency shear-wave data and demonstration in a phantom, human kidneys, and brain. *Magn Reson Med.* 2022;88:1840-1850.
33. Ashburner J. Computational anatomy with the SPM software. *Magn Reson Imaging.* 2009;27:1163-1174.
34. Donoho DL, Johnstone IM, Kerkyacharian G, Picard D. Wavelet shrinkage: asymptopia? *J R Stat Soc Series B Stat Methodol.* 1995;57:301-337.
35. Wagner M, Corcuera-Solano I, Lo G, et al. Technical failure of MR elastography examinations of the liver: experience from a large single-center study. *Radiology.* 2017;284:401-412.
36. Yin M, Glaser KJ, Talwalkar JA, Chen J, Manduca A, Ehman RL. Hepatic MR elastography: clinical performance in a series of 1377 consecutive examinations. *Radiology.* 2016;278:114-124.
37. Joshi M, Dillman JR, Towbin AJ, Serai SD, Trout AT. MR elastography: high rate of technical success in pediatric and young adult patients. *Pediatr Radiol.* 2017;47:838-843.
38. Serai SD, Dillman JR, Trout AT. Spin-echo echo-planar imaging MR elastography versus gradient-echo MR elastography for assessment of liver stiffness in children and young adults suspected of having liver disease. *Radiology.* 2017;282:761-770.
39. Wagner M, Besa C, Ayache JB, et al. MR elastography of the liver: qualitative and quantitative comparison of gradient echo and spin echo echoplanar imaging sequences. *Invest Radiol.* 2016;51:575-581.
40. McIlvain G, McGarry MD, Johnson CL. Quantitative effects of off-resonance related distortion on brain mechanical property estimation with magnetic resonance elastography. *NMR Biomed.* 2022;35:e4616.
41. Peng X, Sui Y, Trzasko JD, et al. Fast 3D MR elastography of the whole brain using spiral staircase: data acquisition, image reconstruction, and joint deblurring. *Magn Reson Med.* 2021;86:2011-2024.
42. Kafali SG, Armstrong T, Shih S-F, et al. Free-breathing radial magnetic resonance elastography of the liver in children at 3 T: a pilot study. *Pediatr Radiol.* 2022;52:1314-1325.
43. Tzschätzsch H. *Quantification of Biophysical Parameters in Medical Imaging.* Springer International Publishing; 2018:281-302.
44. Morr AS, Herthum H, Schrank F, et al. Liquid-liver phantom: mimicking the viscoelastic dispersion of human liver for ultrasound-and MRI-based elastography. *Invest Radiol.* 2022;57:502-509.
45. Yin M, Talwalkar JA, Glaser KJ, et al. Dynamic postprandial hepatic stiffness augmentation assessed with MR elastography in patients with chronic liver disease. *AJR Am J Roentgenol.* 2011;197:64-70.
46. Jajamovich GH, Dyvorne H, Donnerhack C, Taouli B. Quantitative liver MRI combining phase contrast imaging, elastography, and DWI: assessment of reproducibility and postprandial effect at 3.0 T. *PLoS One.* 2014;9:e97355.
47. Tzschätzsch H, Sack I, Garcia SRM, et al. Time-harmonic elastography of the liver is sensitive to intrahepatic pressure gradient and liver decompression after transjugular intrahepatic portosystemic shunt (TIPS) implantation. *Ultrasound Med Biol.* 2017;43:595-600.
48. Guo J, Büning C, Schott E, et al. In vivo abdominal magnetic resonance elastography for the assessment of portal hypertension before and after transjugular intrahepatic portosystemic shunt implantation. *Invest Radiol.* 2015;50:347-351.
49. Perepelyuk M, Chin L, Cao X, et al. Normal and fibrotic rat livers demonstrate shear strain softening and compression stiffening: a model for soft tissue mechanics. *PLoS One.* 2016;11:e0146588.
50. Shahryari M, Keller S, Meierhofer D, et al. On the relationship between metabolic capacities and in vivo viscoelastic properties of the liver. *Front Bioeng Biotechnol.* 2023;10: 1042711. doi:10.3389/fbioe.2022.1042711
51. Tzschätzsch H, Ipek-Ugay S, Guo J, et al. In vivo time-harmonic multifrequency elastography of the human liver. *Phys Med Biol.* 2014;59:1641-1654.

## SUPPORTING INFORMATION

Additional supporting information may be found in the online version of the article at the publisher's website.

**VIDEO S1:** Animations of 100 coronal shear wave speed maps acquired at a frame rate of 62.5 Hz during breathing maneuvers corresponding to Figure 4A of the main manuscript. The left side of the animation shows shear wave speed maps without image registration, while the right side shows maps with image registration. The purple region of interest delineates the liver in the registered images.

**FIGURE S1:** Full set of coronal maps showing shear wave speed during the respiratory study, corresponding to the subset featured in Figure 4A of the main manuscript. 100 liver shear wave speed maps acquired in one subject over 62.5 s were corrected for respiratory motion using image registration. Breathing states are delineated by color-coded frames (green: end-expiration breath-hold;



purple: end-inspiration breath-hold; red: Valsalva; blue: free breathing).

**TABLE S1:** Spatially averaged values of shear wave speed (SWS in m/s) and shear wave amplitude (SWA in  $\mu\text{m}$ ) as well as liver displacement (LD in mm) for different breathing states in the breathing study.

**How to cite this article:** Anders M, Meyer T, Warmuth C, et al. Rapid MR elastography of the liver for subsecond stiffness sampling. *Magn Reson Med.* 2024;91:312-324. doi: 10.1002/mrm.29859